Interactions between Gravity Waves and Planetary-Scale Flow Simulated by the GFDL "SKYHI" General Circulation Model

S. MIYAHARA*

Geophysical Fluid Dynamics Program, Princeton University, Princeton, NJ 08542

Y. HAYASHI AND J. D. MAHLMAN

Geophysical Fluid Dynamics Laboratory/NOAA, Princeton University, Princeton, NJ 08542

(Manuscript received 17 June 1985, in final form 24 February 1986)

ABSTRACT

In order to study interactions between gravity waves and planetary scale flow in the middle atmosphere, a 3° latitude by 3.6° longitude version of the 40-level GFDL "SKYHI" general circulation model is analyzed using bihourly sampled output data.

It is shown by a space–time spectral analysis that gravity waves in the mean zonal westerlies (easterlies) mainly consist of westward- (eastward-) moving components, and carry easterly (westerly) momentum upward, and decelerate the mean zonal westerlies (easterlies) in the mesosphere.

Zonal momentum flux convergence due to gravity waves accounts for nearly all of the Eliassen–Palm (E–P) flux divergence in the summer mesosphere. This convergence accounts for 30%–50% of that in the winter upper mesosphere. However, this percentage is probably an underestimate, since the convergence is significantly enhanced in a high resolution (1° × 1.2°) model currently being integrated.

Vertical propagation of gravity waves is affected not only by the mean zonal wind but also by velocity perturbations associated with planetary waves. The drag force due to gravity waves acts to suppress stationary planetary waves in the winter mesosphere.

1. Introduction

Recently, the importance of drag forces due to internal gravity waves for the middle-atmosphere general circulation has been recognized (see a review by Fritts, 1984). Zonally symmetric models of the middle atmosphere circulation (e.g., Leovy, 1964; Schoeberl and Strobel, 1978; Holton and Wehrbein, 1980) all require a strong Rayleigh friction to obtain realistic mean zonal wind and zonal mean temperature distributions in the mesosphere, namely weak mean zonal wind and a reverse temperature gradient (i.e., the highest temperature at the winter pole and the lowest temperature at the summer pole). It has been hypothesized that the origin of the required Rayleigh friction may be the vertical convergence of eddy momentum flux which occurs when gravity waves break down due to exponential growth of their amplitudes with height (Houghton, 1978; Holton and Wehrbein, 1980).

Lindzen (1981) proposed a simple parameterization of breaking gravity waves which could supply drag forces to decelerate the mean zonal winds in the mesosphere. By introducing the wave-breaking parameterization by Lindzen (1981), Holton (1982) simulated the weak mean zonal winds and the inverse temperature gradient around the mesopause by a mechanistic middle-atmosphere circulation model on a beta plane.

On the other hand, Matsuno (1982) also proposed a parameterization of the vertical convergence of momentum fluxes associated with gravity waves that decay with height due to a permanent eddy diffusion in the mesosphere. A quasi-one-dimensional model of the middle atmosphere incorporating this parameterization could also simulate the weak mean zonal winds and the reverse temperature gradient around the mesopause (Matsuno, 1982).

Holton (1983) and Miyahara (1984) incorporated the effects of gravity waves with a very simplified wave spectrum into mechanistic models of the middle atmosphere circulation based on Lindzen's (1981) and Matsuno's (1982) parameterizations, respectively. The results of these models included a number of features that were in qualitatively good agreement with observations in the mesosphere. Recently, in his numerical experiment on the general circulation of the middle atmosphere, Kida (1984) took into account the effects of randomly prescribed gravity-wave sources at 15 km height. In his model, although any gravity wave breaking or dissipation parameterizations were not used but calculated explicitly, drag forces due to gravity waves

* Permanent affiliation: Department of Physics, Kyushu University, Fukuoka, Japan.

were acting in a way similar to the parameterizations by Lindzen (1981) and Matsuno (1982). Realistic mean zonal wind and zonal mean temperature distributions could be obtained. The success of these models, however, depend greatly on a tuning of internal gravity wave parameters in such a way as to provide appropriate drag forces for producing reasonable mean zonal wind profiles in the mesosphere. Although the values of the gravity wave parameters employed in these models are difficult to verify, these models nevertheless demonstrated the importance of drag forces due to gravity waves for the mesospheric zonal mean circulation.

The possible importance of gravity wave effects on the stratospheric circulation was stressed by Mahlman and Umscheid (1984, hereafter referred to as MU) in connection with the cold polar bias problem from the tropopause to the mesosphere which existed in the 5° lat GFDL "SKYHI" general circulation model (GCM). Based on NMC data, Hamilton (1983) suggested that gravity waves might contribute to a zonal mean decelerative force per unit mass of about 10 m s^{-1}/day at the midlatitude winter stratopause. According to recent radar observations in the mesosphere, gravity waves act to decelerate basic mean zonal winds at the rate of a few tens of meters per second per day (Vincent and Reid, 1983; Fritts et al., 1984).

Interactions between gravity waves and planetary waves have also been discussed in several papers. In Holton's (1983) model a single component of stationary planetary wave was also incorporated in some calculations. The transmission of gravity waves into the mesosphere was greatly affected by mean zonal winds induced by stationary planetary waves. However, his model did not allow a direct interaction between gravity waves and planetary waves. The possible importance of this interaction has been stressed by Lindzen (1984), Schoeberl and Strobel (1984), Dunkerton (1984) and Dunkerton and Butchart (1984). Schoeberl and Strobel (1984) have pointed out the possibility that the parameterized gravity-wave drag force acts like a Rayleigh friction on stationary planetary waves. By introducing Lindzen's (1981) wave-breaking parameterization into a quasi-geostrophic beta plane model, Miyahara (1985) demonstrated that the amplitudes of stationary planetary waves in the mesosphere were greatly suppressed by gravity waves. There is also the possibility that gravity waves indirectly influence the mean zonal fields through increased Eliassen–Palm flux divergence (EPFD) resulting from gravity-wave-induced dissipation of planetary waves.

Lindzen and Tsay (1975) suggested a possible importance of gravity wave effects on the quasi-biennial oscillation of the equatorial stratosphere based on observed data.

Recently, Hayashi et al. (1984) found gravity waves in the equatorial middle atmosphere of the 5° lat version GFDL "SKYHI" GCM in addition to the equatorial Kelvin waves essentially corresponding to those observed. These equatorial gravity waves consist of eastward- and westward-moving components associated with upward fluxes of eastward and westward momentum, respectively. The net convergence of these fluxes in the mesosphere is comparable to or even larger than that due to the Kelvin waves. The analyzed drag force in the equatorial upper mesosphere due to gravity waves is about -2.6 m s^{-1}/day and acts to decelerate the westerlies there. This result is qualitatively consistent with the parameterizations by Lindzen (1981) and Matsuno (1982).

In the present paper we investigate the effects of gravity waves on zonal mean flows and stationary planetary waves in the GFDL "SKYHI" GCM. The model used in the present analysis has a 3° lat by 3.6° long grid mesh with 40 levels in the vertical, with the highest level at about 80 km. Since the present model has a finer horizontal grid system than that analyzed by Hayashi et al. (1984) with 5° × 6° grids, it can resolve shorter scale gravity waves. Unlike mechanistic models (e.g., Holton, 1983; Miyahara, 1984), the GFDL "SKYHI" GCM does not parameterize drag forces due to gravity waves, although it includes a Richardson number dependent eddy vertical diffusion parameterization (see Levy et al., 1982) and a Rayleigh friction for waves only at the top level of the model to prevent a spurious reflection. In the GCM, gravity waves are generated by various mechanisms (e.g., moist convective adjustment, mountains and nonlinear interactions), and the propagation and dissipation of gravity waves are explicitly simulated. It is therefore of interest to evaluate the effects of gravity waves on the middle atmosphere general circulation and to compare them with the effects of parameterized gravity waves. However, the GCM cannot adequately resolve gravity waves with quarter wavelengths smaller than its grid size. The 3° lat model can resolve gravity waves whose horizontal wavelengths are longer than about 1000 km. However, it cannot resolve gravity waves whose vertical wavelengths are shorter than about 20 km in the mesosphere and shorter than about 10 km in the stratosphere. According to recent observations, gravity waves are associated with horizontal scales of less than 100 km (Vincent and Reid, 1983) as well as longer than 1000 km (Fritts et al., 1984; Maekawa et al., 1984). Observations (see the review by Fritts, 1984) also show the presence of mesospheric gravity waves with vertical wavelength less than 20 km. These observations show that the resolution of the present model is not sufficient to resolve the complete gravity wave spectrum in the atmosphere. However, it is of interest to analyze how gravity waves are acting in the limited resolution of the present model.

The conclusions reached through this procedure will be tested against a preliminary analysis of a much higher horizontal resolution (1° lat by 1.2° long) version of the same "SKYHI" GCM.

In section 2 the data used are briefly described. In section 3 a space–time spectral analysis and interactions between gravity waves and mean zonal winds are presented. In section 4 interactions between gravity waves and stationary planetary waves are analyzed. Section 5 gives conclusions and remarks.

2. Data source used in the analysis

In the present study, a 3° lat by 3.6° long version of the GFDL "SKYHI" GCM with Northern Hemisphere winter conditions is analyzed. Details of the GCM are described in Fels et al. (1980), Levy et al. (1982), Andrews et al. (1983) and MU. The output data are sampled bihourly in order to resolve gravity waves. Since the typical periods of gravity waves in this model are 0.5–1.0 day, this sampling interval is more than sufficient.

In order to study the wavenumber–frequency distributions and propagation direction of gravity waves, a space–time spectral analysis is made by use of the lag correlation method (see Hayashi, 1982, for a review of the method). To investigate interactions between gravity waves and planetary scale flow, we also calculate global distributions of the vertical flux of zonal momentum and its convergence due to gravity waves.

The wavenumber–frequency analysis is conducted over the simulated period, 15 December 1983–31 January 1984. The global analysis of momentum flux and its convergence is conducted over two separate periods of 15 December 1983–3 January 1984 (PI) and 26 January–14 February 1984 (PII). Period PI is before a sudden warming type event which began on 14 January 1984, and PII is after the peak of that event. As shown by MU, the simulated magnitude of zonal mean winds in the winter middle atmosphere is considerably stronger before the sudden warming than after it. Since gravity wave momentum fluxes greatly depend on the magnitude of the mean flow (Lindzen, 1981; Matsuno, 1982), it is of interest to investigate the effects of gravity waves on the planetary scale flows in these two different mean states.

A preliminary analysis of the 1° lat model is conducted over the simulated period of 13–22 November 1982 by the use of trihourly data.

3. Zonally averaged properties of gravity waves

In this section we present the results of the wavenumber–frequency analysis and the global distributions of zonally averaged momentum flux and its convergence due to gravity waves.

a. Mean zonal wind

Figures 1a and 1b show the latitude–height distribution of mean zonal wind averaged over the two 20-day periods (PI and PII). The levels of the model are indicated by the standard height corresponding to the model pressure levels.

Compared with the January simulation of MU (5° lat model), the present simulation is more realistic in that the tropospheric maximum westerlies are shifted toward the poles by about 5° and that the equatorial upper tropospheric westerlies are reduced to about 7 m s^{-1}.

In the stratosphere and the mesosphere, the magnitude of the Southern Hemisphere easterlies is realistic up to about 65 km, in both periods. Above this level, the easterlies continue to increase with height up to the top level of the model, contrary to observational results, although the present results are somewhat im-

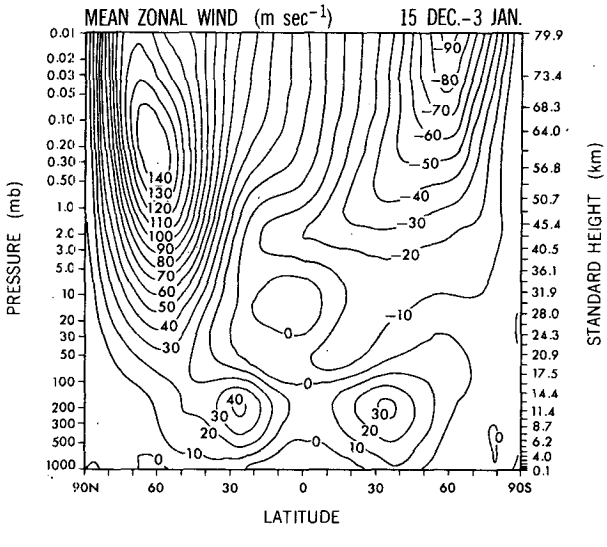

FIG. 1a. Latitude–height distribution of mean zonal wind (m s^{-1}) averaged over the PI period. The standard height indicates the level of the finite-difference model.

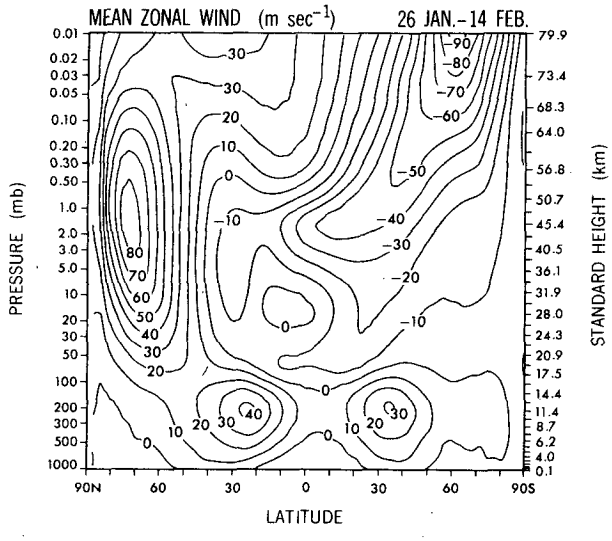

FIG. 1b. As in Fig. 1a except for the distribution in the PII period.

proved over those of MU in that the magnitude of the easterlies is about 10 m s^{-1} weaker.

The maximum of the polar night jet in the PI period is about 140 m s^{-1} around 60 km and 60°N. In the PII period it is about 80 m s^{-1} around 50 km and 70°N. Although the jet is too strong compared to that observed, the simulated jet in both the periods is closed off and the magnitude of the westerlies is 40–60 m s^{-1} weaker than that in MU.

b. Space–time spectral analysis of mean zonal momentum flux

In order to see the behavior of small-scale motions in the model, the vertical pressure velocity ω is analyzed. Figure 2 shows the time–height distribution (15 December 1983–8 January 1984) of ω at 46.5°N and 0° long of the 3° lat model. In the stratosphere and the mesosphere, a downward phase propagation of disturbances whose periods are about 0.5 d can be seen. Vertical wavelengths inferred from the phase tilt are several tens of kilometers. This phase propagation is consistent with upward energy propagation of internal gravity waves. The present model does not have an externally forced diurnal cycle, so that tidal oscillations are not included. On the other hand, in the troposphere, disturbances whose period are longer than a few days can be found. The phase propagation is not as clear as in the stratosphere and mesosphere. These tropospheric disturbances may be associated with baroclinic waves.

The preceding result shows that upward-propagating internal gravity waves definitely exist in the model stratosphere and the mesosphere. To study the wavenumber–frequency distributions and zonal propagation direction of gravity waves, a space–time spectral analysis is made of the vertical flux of zonal momentum $(-\overline{u'\omega'}^{\lambda})$, where u' is the zonal velocity perturbation, and $(\overline{\ }^{\lambda})$ denotes the zonal mean.

Although, an E–P flux analysis is more relevant to the mean zonal momentum flux (Andrews and McIntyre, 1976; Andrews et al., 1983; Hayashi, 1985), in the present paper we shall use $-\overline{u'\omega'}^{\lambda}$ to discuss the zonal momentum flux associated with gravity waves. The reason why we use $-\overline{u'\omega'}^{\lambda}$ instead of the E–P flux is as follows. If we use the E–P flux, it is difficult to isolate the E–P flux due to gravity waves from that due to planetary waves, because of the heat flux term in the vertical component of the E–P flux, which is dominant in case of planetary waves. For gravity waves whose Doppler-shifted periods are much shorter than the Coriolis period, the effect of the heat flux term in the E–P flux is negligible. In the present model, the effect is not crucial for the gravity waves whose zonal wavenumber k is larger than 5 (for detail see the Appendix).

Figure 3 shows the zonal wavenumber–frequency spectral distributions ($1 \leq k \leq 50$, period ≥ 0.167 d) of the vertical flux of zonal momentum $(-\overline{u'\omega'}^{\lambda})$ at 46.5°N (Fig. 3a) and 46.5°S (Fig. 3b) at the 70.6 km level averaged over simulated 15 December 1983—31 January 1984. At 46.5°N westward-moving waves are dominant and carry easterly momentum upward. The dominant period is about 0.5–1.0 d for all wavenumbers, and the dominant phase velocity (relative to the ground) is about -10 m s^{-1} at $k \sim 40$ and about -40

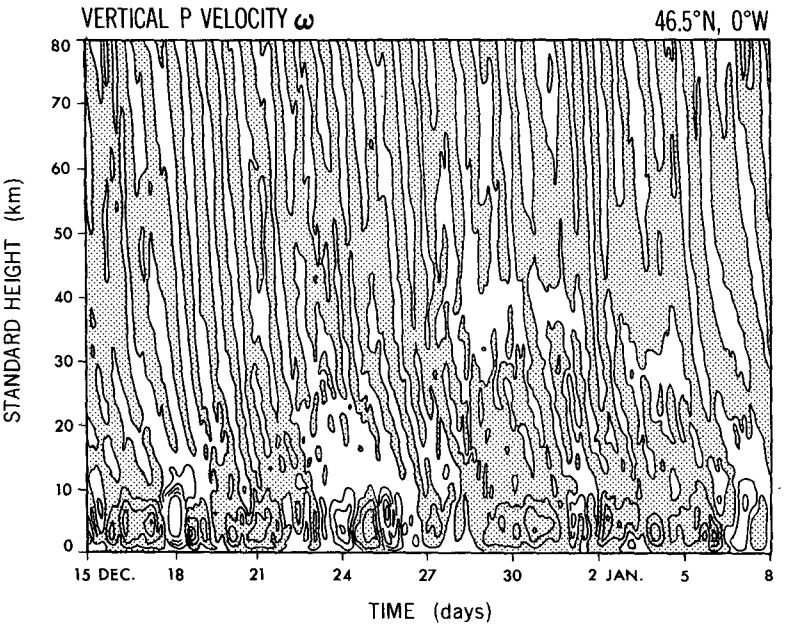

FIG. 2. Time–height distribution of the vertical pressure velocity at 46.5°N and 0° long from 15 December 1983 to 8 January 1984. Positive values are shaded.

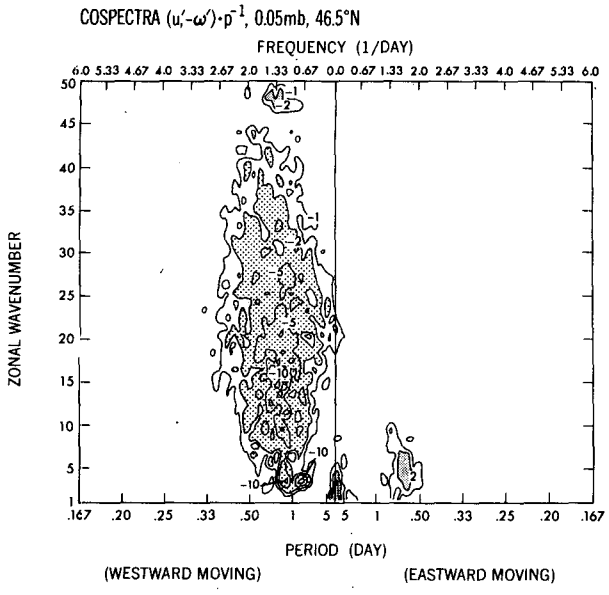

FIG. 3a. Zonal wavenumber–frequency spectral distribution (zonal wavenumber $1 \leq k \leq 50$, period ≥ 0.167 days) of the cospectral density (10^{-6} m s^{-2} d) of the vertical flux of zonal momentum ($-\overline{u'\omega'}^{\lambda} p^{-1}$) at 0.05 mb (70.6 km) at 46.5°N.

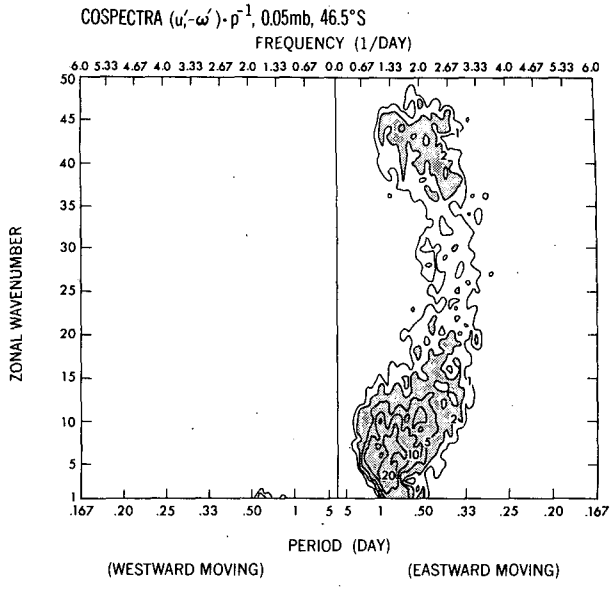

FIG. 3b. As in Fig. 3a except for the distribution at 46.5°S.

m s^{-1} at $k \sim 10$. However, it should be noted that the invariability of the period with wavenumbers might be attributable to the coarse horizontal resolution of the present model. Coarse resolution models have a tendency to predict wave periods longer than their actual periods. According to Kurihara (1965), the simulated periods in the present model are about 110%, 130%, 250% and 420% of the actual wave periods of zonal wavenumber $k = 10$, 20, 30 and 40 waves, respectively. The range of vertical wavelength in the mesosphere as inferred from the dispersion relation of gravity waves is 20–50 km when the Doppler effect is taken into account. This is consistent with the time–height distribution of ω. The correspondence between the signs of relative phase velocity and the momentum flux is consistent with upward-propagating internal gravity waves. It should be noted that the flux due to eastward-moving gravity waves is an order of magnitude smaller than that due to westward-moving gravity waves. The momentum flux associated with low wavenumber components whose period is longer than five days is probably due to planetary waves.

On the other hand, at 46.5°S, eastward-moving waves are dominant and carry westerly momentum upward, and the momentum flux due to westward-propagating waves is negligibly small. The momentum flux due to longer period waves with small zonal wavenumber ($k = 1$–5) is absent, since planetary waves do not exist in the model summer stratosphere and mesosphere where easterlies prevail.

Since internal gravity waves moving against the basic zonal mean winds are shown to be dominant, it is suggested that a selective transmission of internal gravity waves occurs by the Doppler effect of the mean westerlies and easterlies in the winter and summer hemispheres, respectively. This is consistent with the fact that the waves with smaller Doppler-shifted frequencies are preferably dissipated (Matsuno, 1982).

Table 1 shows height distributions of the vertical flux of zonal momentum $-\overline{u'\omega'}^{\lambda}$, consisting of

TABLE 1. Height distributions (46.5°N,S) of the vertical eddy momentum flux $-\overline{u'\omega'}^{\lambda}$ (zonal wavenumbers 5–50) in units of 10^{-5} m s^{-1} mb s^{-1}. The total flux consists of stationary (48-day mean) and transient (deviation from 48-day mean) distributions.

Level (Standard height) (km)	Total at 46.5°N		Total at 46.5°S	
	Stationary	Transient	Stationary	Transient
76.1	−0.000	−0.59	0.000	0.60
70.6	−0.001	−1.16	0.000	1.37
66.0	−0.002	−1.38	0.000	1.48
62.0	−0.002	−1.61	0.000	1.44
58.5	−0.001	−1.74	0.000	1.40
52.5	−0.017	−1.89	0.000	1.33
46.6	−0.027	−2.12	0.000	1.15
41.7	0.004	−2.43	0.000	0.99
37.1	−0.003	−2.79	0.000	0.74
32.9	−0.015	−3.10	−0.000	0.58
29.0	−0.009	−3.58	0.000	0.28
25.2	0.045	−4.07	0.001	−0.18
21.7	0.258	−4.70	0.008	−0.74
18.3	0.629	−5.09	0.112	−0.68
15.2	0.936	−4.26	0.396	2.09
12.2	0.800	−2.75	2.765	−13.76
9.4	−3.271	−68.02	6.509	−182.97
6.8	−6.802	−215.38	5.786	−294.04
4.5	−1.863	−219.91	3.754	−221.91
2.5	−2.736	−155.41	3.225	−142.53

higher zonal wavenumber components (k = 5–50) at 46.5°N,S. Since planetary waves in the stratosphere and the mesosphere mainly consist of lower zonal wavenumbers, the wavenumber components k = 1–4 are eliminated in an effort to reduce planetary waves. The total flux consists of stationary (48 day mean) and transient (deviations from 48 day mean) distributions. The momentum flux associated with transient components is dominant over stationary components at all heights at both latitudes. It should be remarked that the present model does not resolve small-scale stationary mountain waves that would also contribute to vertical momentum flux. The transient distributions are further separated into eastward- and westward-moving components. Figure 4 shows height distributions of the vertical fluxes of zonal momentum $-\overline{u'\omega'}^{\lambda}$ (k = 5–50), consisting of westward- and eastward-moving components, respectively. Throughout the stratosphere and the mesosphere, westward-moving waves carry easterly momentum upward and eastward-moving waves carry westerly momentum upward. These results indicate that these momentum fluxes are mainly due to internal gravity waves propagating upward through the stratosphere and the mesosphere. Above 12 km at 46.5°N, the easterly (negative) momentum flux due to westward-propagating waves is dominant. Above 30 km, in particular, this easterly flux is an order of magnitude larger than the westerly flux due to eastward-moving waves. At this latitude, mean zonal winds are westerly at all levels, so that westward-moving waves and fast eastward-moving waves (see Fig. 2a) can propagate into the upper layers, while slow eastward-moving waves cannot propagate into the upper layers due to critical level type absorption and/or thermal dissipation (Matsuno, 1982; Schoeberl and Strobel, 1984; Fels, 1984).

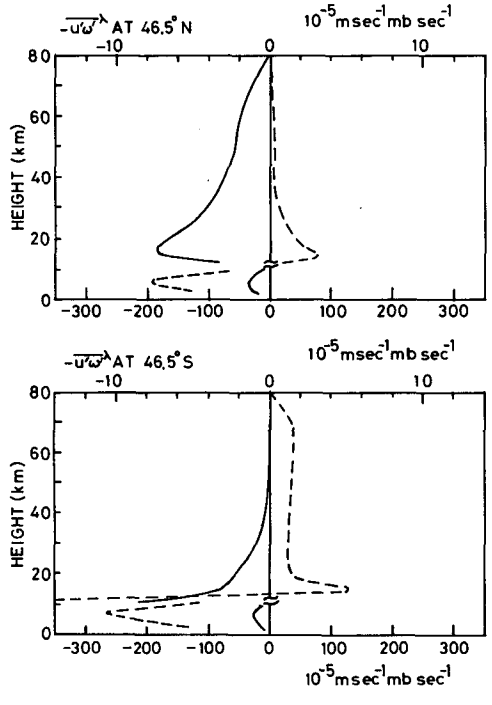

FIG. 4. Height distribution (46.5°N,S) of the vertical eddy momentum fluxes $-\overline{u'\omega'}^{\lambda}$ (zonal wavenumbers 5–50), consisting of westward- (solid line) and eastward- (dashed line) moving components.

At 46.5°S the westerly (positive) momentum flux due to eastward-moving waves is dominant above 30 km, while the easterly momentum flux due to westward-moving components is as large as the westerly momentum flux at the levels 18–25 km. The mean zonal winds at this latitude are westerly below 20 km, and easterly above 20 km. Thus, westward-moving gravity waves that propagate from the troposphere may encounter critical levels at some heights in the stratosphere and be inhibited from propagating into the upper layers.

These results demonstrate a very distinct selective transmission of gravity waves in the present model, as expected on theoretical grounds (Lindzen, 1981; Matsuno, 1982).

In the troposphere, the momentum flux due to eastward-moving waves is easterly and an order of magnitude larger than the easterly momentum flux due to westward-moving waves at both latitudes. This suggests that the eastward-moving waves cannot be interpreted as gravity waves. According to a space–time spectral analysis (not illustrated), these tropospheric eastward-moving waves have their spectral peak at longer period (longer than two days). Thus, the easterly momentum flux in the troposphere is interpreted as being due to baroclinic waves.

Figure 5 shows the vertical profiles of the vertical convergence of the mean zonal momentum flux ($-\partial\overline{u'\omega'}^{\lambda}/\partial p$) above 20 km at 46.5°N,S. At 46.5°N easterly acceleration due to westward-moving waves is dominant in the mesosphere with the maximum value of 30×10^{-5} m s^{-2} at the top level, while westerly acceleration due to eastward-moving waves is dominant in the upper mesosphere at 46.5°S. This result shows that selectively propagating gravity waves act significantly to decelerate the mean zonal winds in the upper mesosphere in the present model. The result is in qualitatively good agreement with the theoretical works of Lindzen (1981) and Matsuno (1982). However, it should be cautioned that the present model has strong Rayleigh friction (9.26×10^{-4} s^{-1}) only for waves at the top level of the model (about 80 km height) in order to prevent a spurious reflection. Thus there is the possibility that the momentum convergence due to wave dissipation above 75 km may be partly spurious. The model vertical convergence in the stratosphere at 46.5°N is smaller than 0.5×10^{-5} m s^{-2} and plays a less important role than the EPFD due to planetary waves (see Fig. 7c and 8c). At 46.5°S, the vertical divergence of the eastward-moving components at 30–60 km is comparable to or smaller than that of the

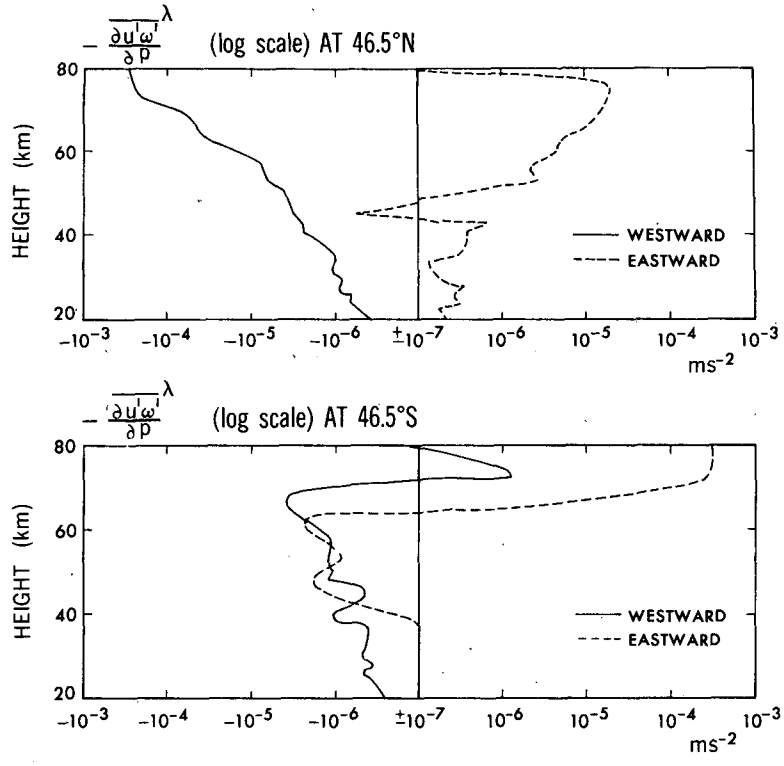

FIG. 5. Vertical distributions of the convergence of the vertical flux of momentum due to higher wavenumber components (zonal wavenumbers 5–50) at 46.5°N (top) and at 46.5°S (bottom). The solid line indicates westward-moving components, while the dashed line indicates eastward-moving components.

westward-moving components, although the vertical flux of the eastward-moving waves is larger than that of the westward-moving waves (Table 1). This is because the westerly momentum flux carried by the eastward-moving waves slightly increases with height between 37 and 66 km. As will be shown later, this increase is due to eastward-moving waves that propagate meridionally from the low latitudes through the low latitude easterlies.

It is of interest to compare the preceding results to those in the tropics. Table 2 shows the height distributions of the vertical flux of zonal momentum at 1.5°N. Momentum fluxes associated with transient components are dominant at all levels, although the stationary momentum flux is not negligible in the lower troposphere (<5 km). Figure 6 shows the height distributions of the vertical fluxes of zonal momentum at 1.5°N, consisting of westward- and eastward-moving components, respectively. In constrast to the midlatitudes, momentum fluxes associated with westward- and eastward-moving components are of the same order of magnitude at all heights. This means that transmissivities of the eastward- and westward-propagating gravity waves are not as very different from each other as in the case of midlatitudes, because mean zonal winds in the equatorial region are not as strong as in the midlatitudes. However, the momentum flux due to eastward-moving components is systematically larger than that due to westward-moving components above 18 km, due to the existence of mean zonal easterlies. The

TABLE 2. As in Table 1 except for the distributions at 1.5°N.

Level (Standard height) (km)	Stationary	Transient
76.1	0.000	0.030
70.6	0.000	0.165
66.0	0.002	0.474
62.0	0.001	0.962
58.5	0.001	1.530
52.5	0.001	2.767
46.6	−0.002	3.460
41.7	0.003	3.590
37.1	0.006	3.111
32.9	−0.003	3.213
29.0	−0.002	4.192
25.2	−0.003	7.669
21.7	−0.004	10.282
18.3	0.051	11.829
15.2	−0.594	11.731
12.2	−2.652	−4.577
9.4	2.713	−37.219
6.8	10.872	−21.832
4.5	16.020	4.994
2.5	−13.900	4.516
1.0	10.265	55.219

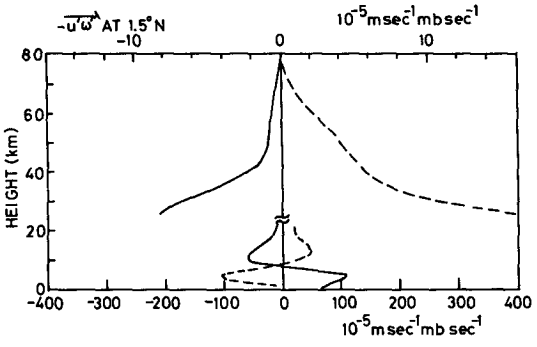

FIG. 6. As in Fig. 4 except for the distributions at 1.5°N.

difference of the momentum fluxes between eastward-moving and westward-moving components above 30 km in the present model is larger than that in the previous model (Hayashi et al., 1984) using annual mean insolation conditions. The westward- and eastward-moving components reverse the sign of their vertical momentum flux at 8 km as in Hayashi et al. (1984). This suggests that these equatorial gravity waves are mainly generated due to convective adjustment around this level and propagate upward and downward.

c. *Zonally averaged momentum flux and its convergence due to gravity waves*

As shown in section 3b, gravity waves in the present model have a very distinct selective transmission at 46.5°N,S in the stratosphere and mesosphere and significantly act to decelerate mean zonal wind in the mesosphere. It is also shown that significant amounts of eastward- and westward-moving gravity waves exist in the equatorial region.

In this subsection, the global distribution of zonally averaged momentum flux and its convergence due to gravity waves are discussed.

In order to remove the momentum flux due to planetary waves, we use only a space filter. As shown in section 3b, momentum flux consisting of higher wavenumber components ($k \geqslant 5$) in the stratosphere and the mesosphere can be interpreted as being mainly due to internal gravity waves. Hereafter in the present paper, to eliminate momentum fluxes due to planetary waves, higher wavenumber components ($5 \leqslant k \leqslant 50$, $5 \leqslant l \leqslant 50$) are used to calculate the momentum flux, where k and l are the zonal and meridional Fourier wavenumbers, respectively. In a trial calculation we used higher wavenumber components ($10 \leqslant k \leqslant 50$, $10 \leqslant l \leqslant 50$). However, the results in the stratosphere and the mesosphere are qualitatively similar, and the magnitudes of momentum fluxes are about two-thirds of the present truncation results.

Figure 7a shows the latitude–height distribution of $-\overline{u'\omega'}^{\lambda}$ averaged over the PI period. In the middle to high latitudes of the troposphere in both Northern and Southern hemispheres, there exist regions of large negative fluxes (i.e., upward transport of eastward momentum). These large negative fluxes are due to eastward-propagating baroclinic waves, as was shown in section 2. Even if we had used a space–time filter, it would be still difficult to isolate the gravity waves from the baroclinic waves, because the baroclinic wave spectrum spreads from low to high frequencies. In the Northern Hemisphere the negative flux continues into the upper mesosphere through the westerlies (see Fig. 1) in the middle atmosphere. On the other hand, in the Southern Hemisphere the negative flux is confined below 30 km. As was shown in section 2, these negative fluxes are due to westward-moving gravity waves whose propagation is blocked by the easterlies in the summer stratosphere, whereas the westward-moving gravity waves in the Northern Hemisphere can propagate into the upper mesosphere through the westerlies. In the easterlies in the summer stratosphere and mesosphere, the flux is positive (i.e., upward transport of westerly momentum) due to eastward-moving gravity waves.

Figure 7b shows the latitude–height distribution of the vertical convergence of the momentum flux $(-\partial\overline{u'\omega'}^{\lambda}/\partial p)$ averaged over the PI period. In the winter mesosphere, divergence occurs with a maximum magnitude of -30×10^{-5} m s^{-2}, which significantly acts to decelerate the background westerlies. On the other hand, in the summer hemisphere convergence occurs with almost the same magnitude, which also acts to decelerate the background easterlies. Since the effect of radiative damping of gravity waves is negligible for long vertical wavelength (Fels, 1984, 1985), this momentum deposition is mainly due to the model Richardson-number dependent vertical eddy diffusion (Levy et al., 1982), which parameterizes the effects of breaking unstable waves. The direct effect of the vertical diffusion on the zonal mean winds is one order smaller than the momentum deposition by the breaking gravity waves. These properties of gravity wave effects are in qualitative agreement with the theoretical works of Lindzen (1981), Holton (1982) and Matsuno (1982). At the stratopause, maximum magnitude of the convergence is 0.5×10^{-5} m s^{-2}, while in the stratosphere, the magnitudes are about 0.1×10^{-5} m s^{-2}. In the midlatitude upper troposphere, the convergence is about -1×10^{-5} m s^{-2} in both hemispheres.

Figure 7c shows the latitude–height distributions of the direction and magnitude of the E–P flux divided by pressure and EPFD, consisting of all wavenumber components averaged over the PI period before the sudden warming. A careful inspection of the normalized E–P flux vectors reveals their constancy with height in the mesosphere. This suggests that wave saturation occurs there. In the Northern Hemisphere, the total EPFD is predominant over gravity wave momentum flux convergence except in the upper mesosphere. This predominance means that the total EPFD is mostly due to planetary waves and that the effects of gravity waves are negligible at these heights in the present

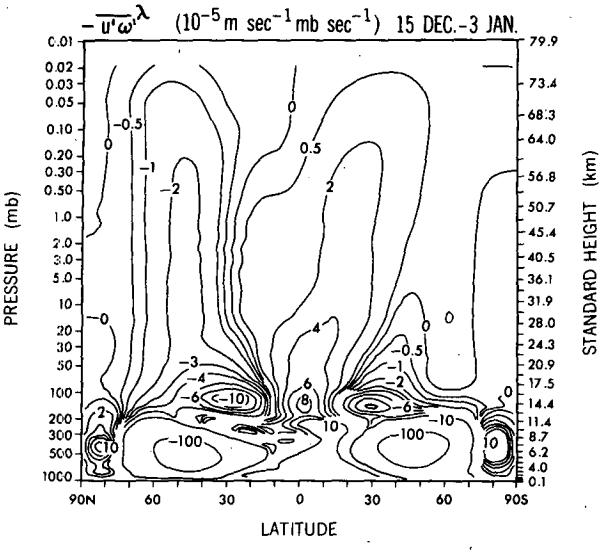

FIG. 7a. Latitude–height distribution of $-\overline{u'\omega'}^{\lambda}$ (10^{-5} m s^{-1} mb s^{-1}) consisting of higher wavenumber components ($5 \leq k \leq 50$, $5 \leq l \leq 50$).

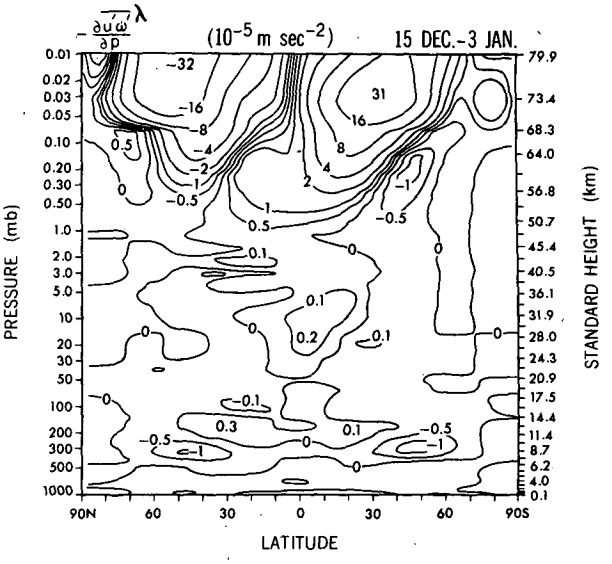

FIG. 7b. Latitude–height distribution of the convergence of vertical eddy momentum flux $-\partial\overline{u'\omega'}^{\lambda}/\partial p$ (10^{-5} m s^{-2}).

model. This result indicates that the deceleration effects of gravity waves in the model stratosphere and lower mesosphere are smaller than those in the real atmosphere, which is estimated at about 10×10^{-5} m s^{-2} at the middle latitude winter stratopause (Hamilton, 1983; Smith and Lyjak, 1985). In the midlatitude upper mesosphere, however, the model gravity wave momentum convergence accounts for 30%–50% of the total EPFD. In the summer upper stratosphere and the mesosphere the total EPFD is almost comparable to the vertical momentum convergence due to gravity waves. This justifies the neglect of the effects of the horizontal momentum flux and the heat flux due to gravity waves in the present analysis. These results show that the gravity wave momentum convergence plays an important role in the model's upper mesosphere. However, the magnitude of the deceleration effects in the present model still seems to be insufficient to realize a realistic mean zonal-wind distribution in the stratosphere and mesosphere. This insufficiency is probably attributable to the lack of small-scale gravity waves, which are not resolved in the present model.

During the sudden warming period, the EPFD due to planetary waves becomes temporarily large as in MU (1984). The mean zonal wind is reduced to 80 m s^{-1} at the winter lower mesosphere, as a result of the warming. It is of interest to analyze the gravity wave momentum flux in the reduced mean zonal wind.

Figures 8a and 8b show the latitude–height distributions of filtered $-\overline{u'\omega'}^{\lambda}$ and $-\partial\overline{u'\omega'}^{\lambda}/\partial p$ averaged over the PII period. These distributions are qualitatively similar to those in the PI period. The negative flux in the winter stratosphere and the mesosphere is somewhat weaker than that in the PI period. The difference of magnitude may be due to the difference of transmissivity of gravity waves. In the PII period the magnitude of the polar night jet is considerably smaller than that in the PI period (see Figs. 1a and 1b). Thus, transmissivity of gravity waves in the PII period is less than that in the PI period, because the relative phase velocity of westward-moving gravity waves is smaller than that in the PI period. The convergence of this smaller flux in the upper mesosphere (the maximum magnitude of -9×10^{-5} m s^{-2}) is also smaller than that in the PI period. Since the sudden warming did not affect the Southern Hemisphere, the zonal mean

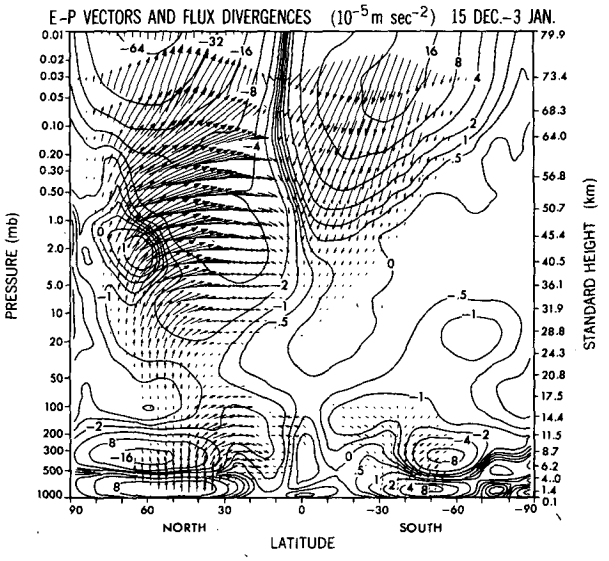

FIG. 7c. Latitude–height distributions of Eliassen–Palm flux vector divided by pressure and its divergence (EPFD) (10^{-5} m s^{-2}) consisting of all wavenumber components averaged over the PI period.

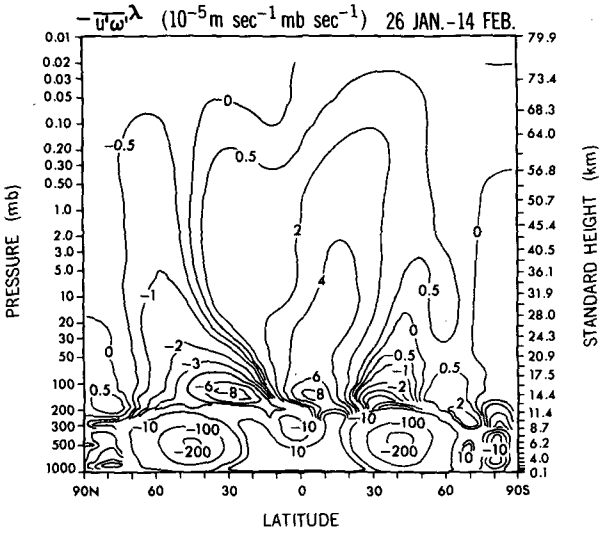

FIG. 8a. As in Fig. 7a except for the distribution in the PII period.

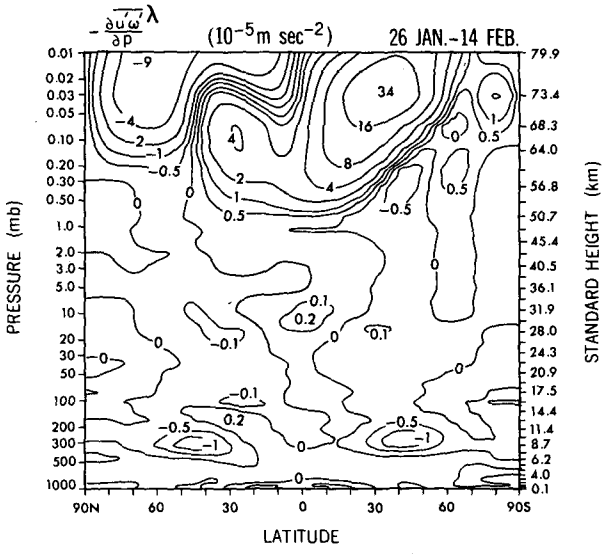

FIG. 8b. As in Fig. 7b except for the distribution in the PII period.

wind and the momentum convergence did not change significantly from PI to PII.

Figure 8c shows the latitude–height distributions of the direction of E–P flux and its divergence, consisting of all wavenumber components averaged over the PII period. The magnitude of the EPFD in the northern upper mesosphere is almost half that in the PI period, while the magnitude is almost the same in the stratosphere and the lower mesosphere (Fig. 7c). This small EPFD in the upper mesosphere in this period is mainly caused by the decrease of the zonal momentum flux convergence due to gravity waves.

d. Preliminary analysis of a high resolution model

Recently preliminary results have been available from a current "SKYHI" (1° lat by 1.2° long) model which has three times finer horizontal resolution than the 3° lat model. The model has not yet run in mid-winter, but it has run in November. Although the period is different, it is of interest to compare the results with those of the 3° lat model.

Figure 9 shows the latitude–height distribution of the mean zonal wind averaged over the simulated period of 13–22 November 1982. In the middle to high latitudes of the stratosphere and the mesosphere of the Northern Hemisphere, the polar night jet exists with the maximum speed of 90 m s^{-1} and is closed off in the upper mesosphere. In the Southern Hemisphere, westerlies still remain with the maximum speed of 40 m s^{-1}, and is closed off. The magnitudes of these westerlies in the mesosphere are about 50 m s^{-1} weaker than those of the same period simulated by the 3° lat model. In the stratosphere of the equatorial region, easterlies of −20 m s^{-1} are present that connect to the forming summer easterlies in the mesosphere.

Figure 10a shows the latitude–height distributions of $-\overline{u'\omega'}^{\lambda}$ in the same period. In this analysis, zonal wavenumber components ($5 \leqslant k \leqslant 150$) are used to calculate the momentum flux. The meridional wavenumber is not truncated. The results are, however, not seriously affected by including the meridional wavenumber components $l \leqslant 4$, as will be shown later. In the stratosphere and the mesosphere, the momentum fluxes are negative (positive) in the westerlies (easterlies), as is the case with the 3° lat model. However, the magnitude of the momentum flux of the 1° lat model is two to three times larger than that in the PI period, or about five times larger than that in the PII period

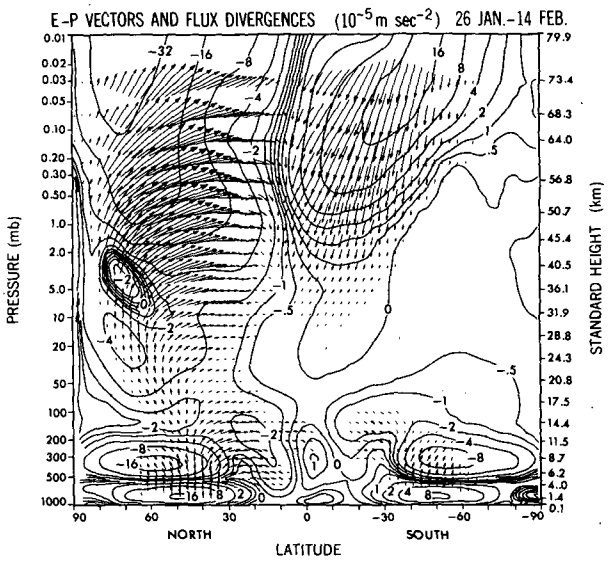

FIG. 8c. As in Fig. 7c except for the distributions in the PII period.

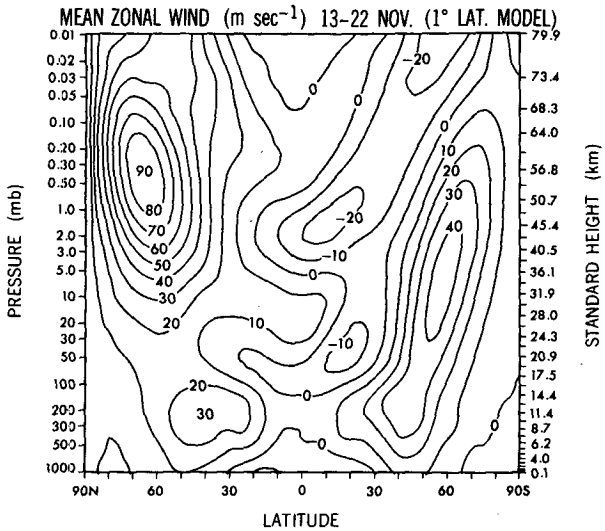

FIG. 9. Latitude–height distribution of mean zonal wind (m s^{-1}) of the 1° lat model averaged over 13–22 November 1982.

of the 3° lat model, while the magnitudes of the mean zonal winds in the Northern Hemisphere (Fig. 9) are smaller than those in the PI period (Fig. 1a) or comparable to those of the PII period (Fig. 1b). The magnitude of the momentum flux in the easterlies is also about two times larger than that of the 3° lat model in spite of the weaker easterlies.

Figure 10b shows the latitude–height distributions of the vertical convergence of the momentum flux $-\partial\overline{u'\omega'}^{\lambda}/\partial p$. The magnitude at 70 km in the midlatitude of the Northern Hemisphere is about three times larger than that of the PI period (Fig. 7b) and about six times larger than that of the PII period (Fig. 8b) of the 3° lat model. The westerly decelerating region is considerably larger than that in the 3° lat model. The -0.5×10^{-5} m s^{-2} line nearly reaches the 1.5 mb level, while in 3° lat cases it is at 0.5 and 0.2 mb levels for the PI and PII periods, respectively. The easterly deceleration in the upper summer mesosphere is almost the same as that in the 3° lat model, in spite of the weaker mean zonal easterlies.

As shown before, the effects of gravity waves in the 1° lat model are certainly greater than those in the 3° lat model. In order to investigate which part of the wave spectrum contributes to the increase of the gravity wave momentum flux, the following analyses are made. Figure 11a shows the latitude–height distributions of the momentum flux consisting of the wavenumber components ($5 \leq k \leq 150$, $5 \leq l \leq 150$) averaged over six sampling times on 13 November. Although the sampling period is much shorter, the result is almost the same as the 9-day mean which consists of wavenumber components ($5 \leq k \leq 150$, all l). This result shows that the contribution of the low meridional wavenumber components ($0 \leq l \leq 4$) is small. Figure 11b shows the latitude–height distributions of the momentum flux consisting of the wavenumber components ($5 \leq k \leq 50$, $5 \leq l \leq 50$). This wavenumber truncation is just the same as the resolvable wavenumbers of the 3° lat model. Compared to the former case, the magnitudes of the fluxes in the westerlies in the middle atmosphere are about two-thirds. However, the magnitudes in low latitudes are not as reduced by the reduction of high wavenumber components. This suggests that a cancellation of the momentum fluxes between eastward- and westward-moving waves occurs in this region because of the weak mean zonal winds,

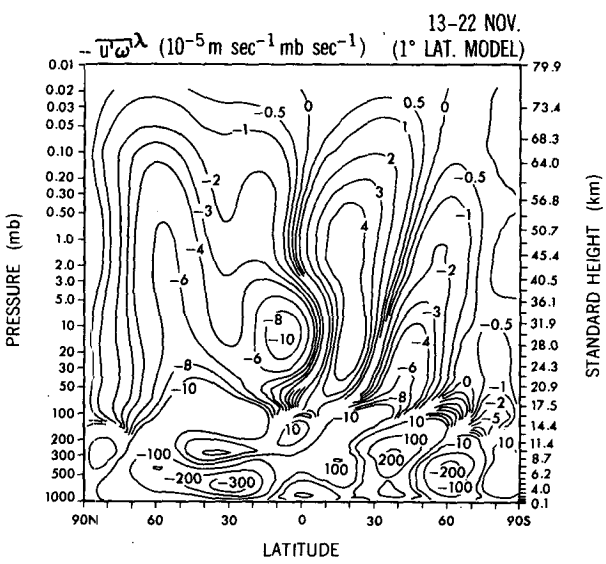

FIG. 10a. Latitude–height distribution of $-\overline{u'\omega'}^{\lambda}$ (10^{-5} m s^{-1} mb s^{-1}) of the 1° lat model, consisting of zonal wavenumber components ($5 \leq k \leq 150$) averaged over 13–22 November 1982.

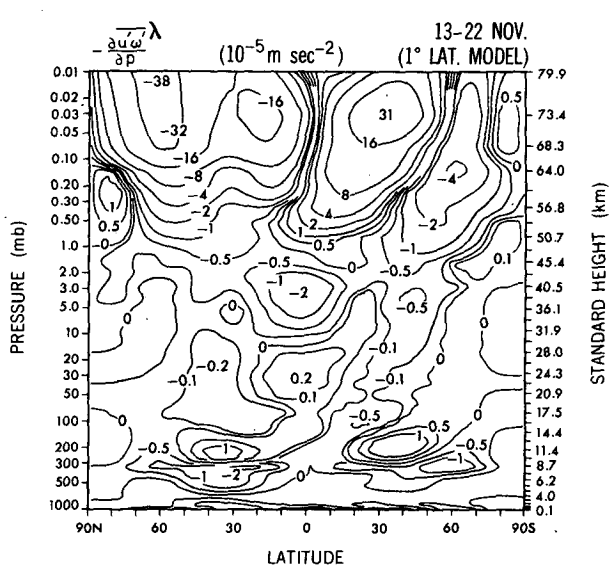

FIG. 10b. Latitude–height distribution of the convergence of vertical eddy momentum flux $-\partial\overline{u'\omega'}^{\lambda}/\partial p$ (10^{-5} m s^{-2}).

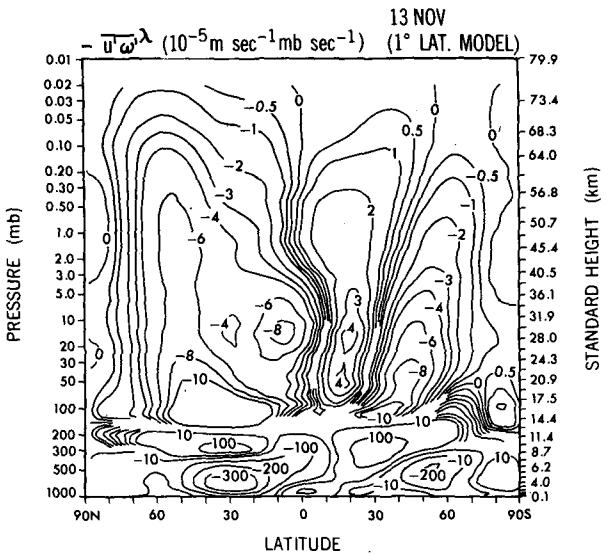

FIG. 11a. Latitude–height distribution of $-\overline{u'\omega'}^{\lambda}$ (10^{-5} m s^{-1} mb s^{-1}) of the 1° lat model, consisting of zonal and meridional wavenumber components ($5 \leq k \leq 150$, $5 \leq l \leq 150$) averaged over six sampling times on 13 November 1982.

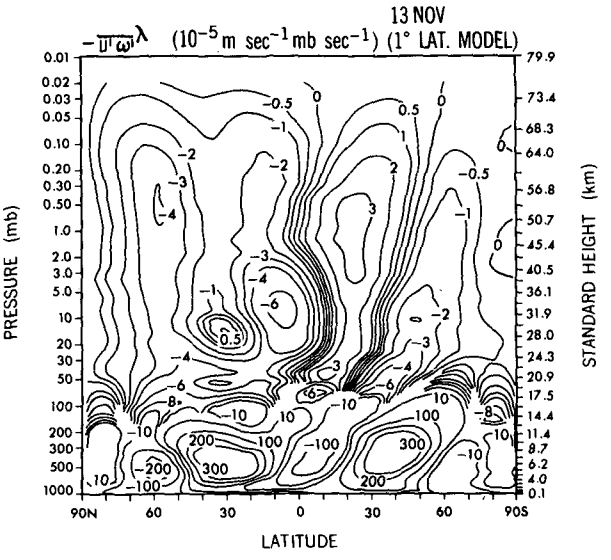

FIG. 11b. As in Fig. 11a except for the difference of the wavenumber truncation ($5 \leq k \leq 50$, $5 \leq l \leq 50$).

while it does not occur in the westerlies in which a strict selective transmission of gravity waves occurs.

It is noteworthy that the magnitude of the momentum flux of the 3° lat model resolution part of the 1° lat model in the polar night jet is significantly larger than that of the 3° lat model (Figs. 7a and 8a). In spite of the difference between the analyzed periods, it is likely that the power of the spectrum of $5 \leq k \leq 50$, $5 \leq l \leq 50$ is increased by including the higher wavenumber components into the model.

4. Interactions between gravity waves and planetary waves

In section 3, it was shown that propagation of gravity waves in the model is greatly affected by mean zonal winds, and that mean zonal winds themselves are affected by gravity waves in a systematic way. Since gravity waves have smaller horizontal scale than planetary waves, propagation of gravity waves is systematically affected not only by mean zonal winds but also by velocity perturbations associated with planetary waves. These affected gravity waves may reciprocally affect the planetary waves (Dunkerton, 1984; Dunk-

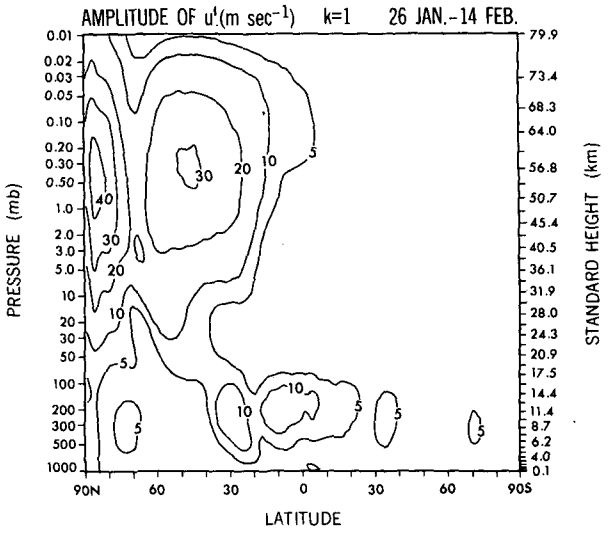

FIG. 12a. Latitude–height distribution of the amplitude of zonal wind perturbation of zonal wavenumber 1 averaged over the PII period.

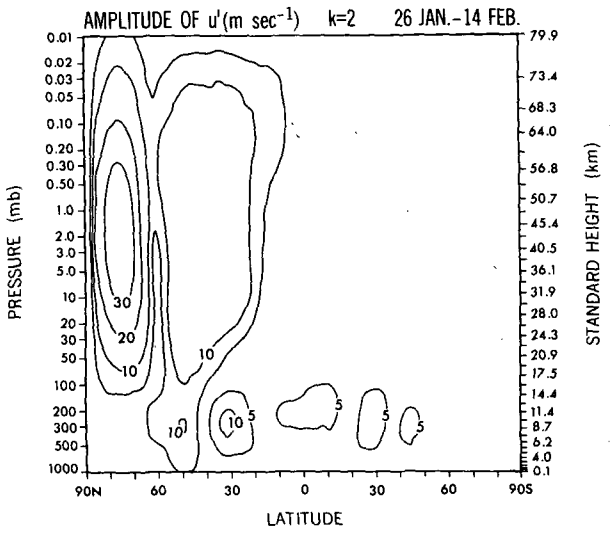

FIG. 12b. As in Fig. 12a except for the distribution of zonal wavenumber 2.

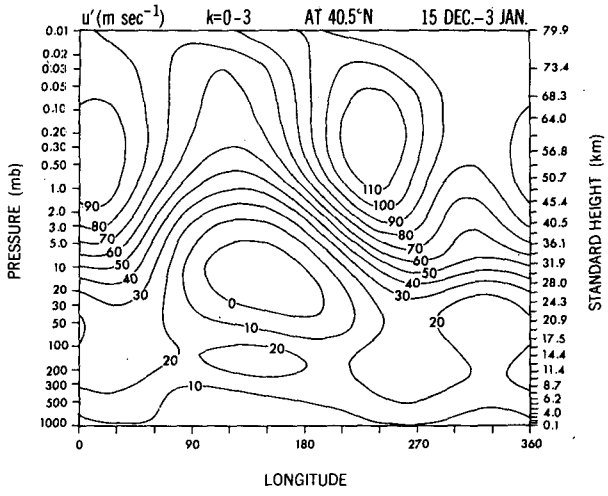

FIG. 13a. Longitude–height cross section (40.5°N) of the time-mean zonal wind consisting of zonal wavenumbers 0–3 averaged over the PI period.

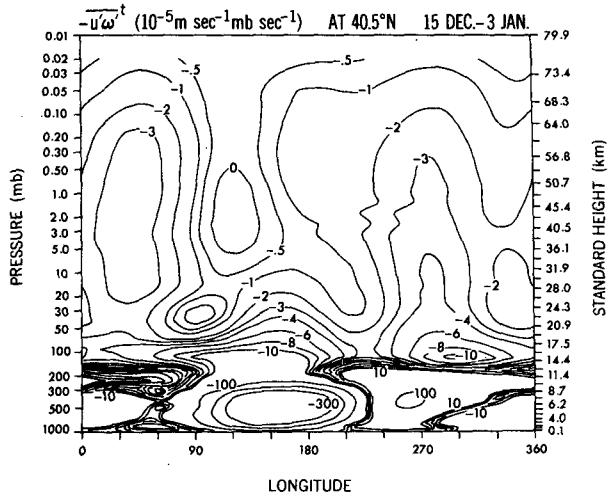

FIG. 13b. Longitude–height cross section (40.5°N) of the wavenumber-filtered (k = 0–3) time-mean vertical flux of zonal momentum due to higher wavenumber components ($5 \leq k \leq 50$, $5 \leq l \leq 50$).

erton and Butchart, 1984; Lindzen, 1984; Schoeberl and Strobel, 1984; Miyahara, 1985). It is also of interest to examine the mutual interactions between gravity waves and planetary waves.

a. Planetary waves

Figures 12a and 12b show the latitude–height distributions of the model amplitudes of zonal wind perturbations of zonal wavenumber 1 and 2, respectively, averaged over the PII period. In the upper troposphere, some maxima can be found, which correspond to activities of midlatitude planetary waves and equatorial waves. In the stratosphere and the mesosphere, wave activity is confined to the winter hemisphere. These waves are mainly quasi-stationary planetary waves. The latitude–height distributions (not illustrated) in the PI period are qualitatively similar to those in the PII period.

b. Correlations between gravity waves and planetary waves

Figure 13a shows the longitude–height cross section (40.5°N) of the time-mean zonal wind consisting of zonal wavenumbers 0–3, while Fig. 13b shows spatially smoothed time-mean vertical flux of zonal momentum due to higher wavenumber components ($5 \leq k \leq 50$, $5 \leq l \leq 50$) for the PI period. The spatial smoothing is accomplished by the wavenumber filter (k = 0–3) in order to examine the effect of gravity waves on the planetary scale flow. At the longitudes where westerlies are strong, the momentum flux is negative and easterly

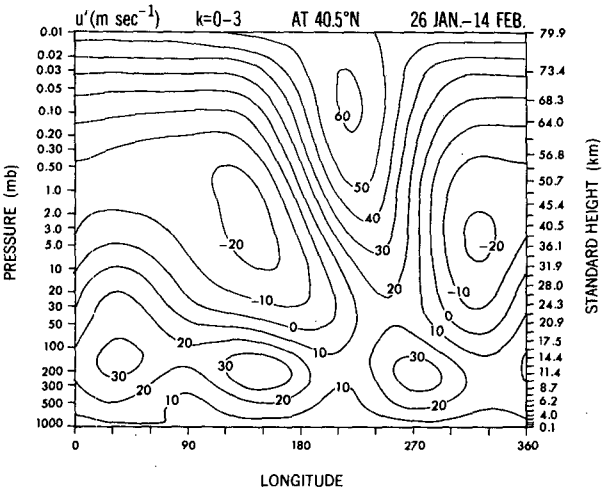

FIG. 14a. As in Fig. 13a except for the PII period.

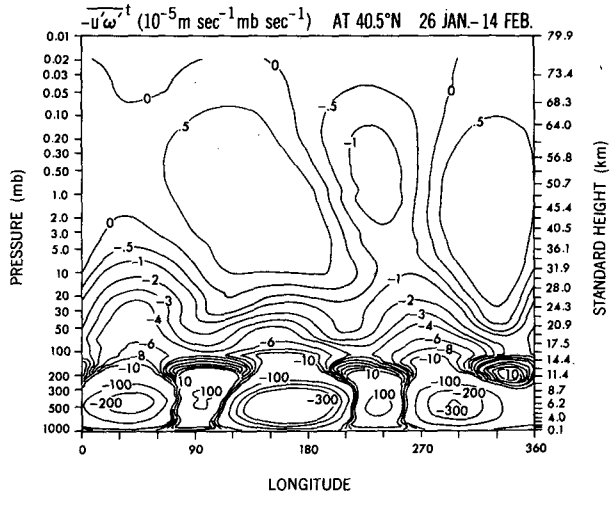

FIG. 14b. As in Fig. 13b except for the PII period.

momentum is carried upward. On the other hand, in the longitudes where westerlies are weak, the momentum flux is also weak. Figures 14a and 14b show the same distributions except for the PII period. In this period easterlies exist in the middle atmosphere associated with planetary waves. At the longitudes where easterlies exist (Fig. 14a) positive (westerly) momentum flux exists (Fig. 14b). These results show that westward-moving gravity waves that carry easterly momentum upward easily propagate in the strong westerly region, while their propagation is blocked in the easterly region. Since zonal mean winds in the PII period are smaller than those in the PI period, the local easterlies and the blocking effect of westward-moving gravity waves can be seen clearly in the PII period. As a result of a cancellation between positive and negative fluxes, the zonal mean flux in the PII period is smaller than that in the PI period, as shown in section 3. Note that the zonal mean flux is small for small zonal mean winds, even if the zonal mean wind results from a cancellation between local westerlies and easterlies.

Figures 15a and 15b are the same as Figs. 14a and 14b except for the longitude–latitude distributions at 73.4 km, and Fig. 15c shows the distribution of vertical convergence of the flux. In the Northern (winter) Hemisphere, the zonal wind has large spatial variations due to planetary waves. The vertical flux of zonal momentum and its convergence also have some spatial variations. In the region where the zonal wind has positive (negative) deviations, the vertical flux of zonal momentum has negative (positive) deviations, and its convergence has negative (positive) deviations. This means that the momentum flux convergence associated with gravity waves acts to suppress stationary planetary waves in the present model. The possibility of such suppression is suggested by theoretical studies (Lindzen, 1984; Schoeberl and Strobel, 1984; Miyahara, 1985). In the PI period (not illustrated), the magnitude of zonal mean westerlies is so strong that the correlation between gravity waves and planetary waves is not so clear as in the PII case. However, we can still recognize a systematic relation between planetary waves and gravity waves in the low to middle latitude region.

In order to see the suppression rate of stationary planetary waves by gravity waves, we define an equivalent Rayleigh friction coefficient for the zonal wind component of planetary waves by the following equation

$$\alpha = -\sum_{k=1}^{3} u_k F_k / \sum_{k=1}^{3} u_k^2, \qquad (1)$$

where u_k is the Fourier coefficient of the time-mean zonal wind for zonal wavenumber k, and F_k is the Fourier coefficient of the vertical flux convergence of zonal momentum due to higher wavenumber components ($5 \leqslant k \leqslant 50$, $5 \leqslant l \leqslant 50$).

Figures 16a and 16b show the latitude–height distributions of the equivalent Rayleigh friction coeffi-

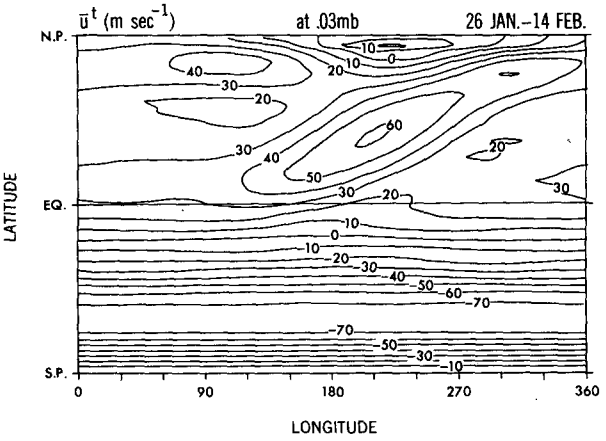

FIG. 15a. Longitude–latitude distribution of the time-mean zonal wind (m s^{-1}) at 0.03 mb, consisting of zonal wavenumbers 0–3 averaged over the PII period.

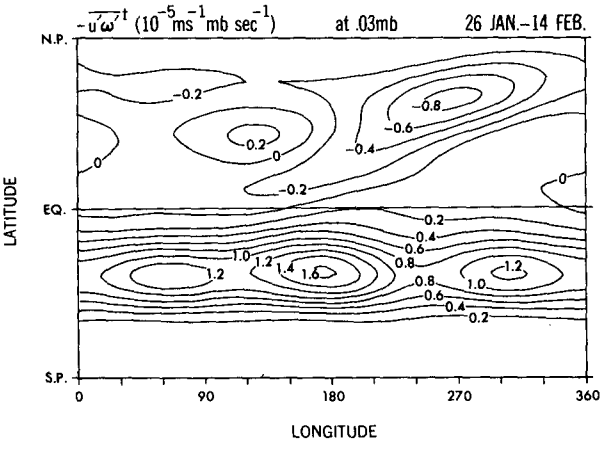

FIG. 15b. Longitude–latitude distribution of spatially smoothed time-mean vertical flux of zonal momentum (10^{-5} m s^{-1} mb s^{-1}) due to higher wavenumber components ($5 \leqslant k \leqslant 50$, $5 \leqslant l \leqslant 50$) at 0.03 mb. The spatial smoothing is accomplished by a wavenumber filter (k = 0–3).

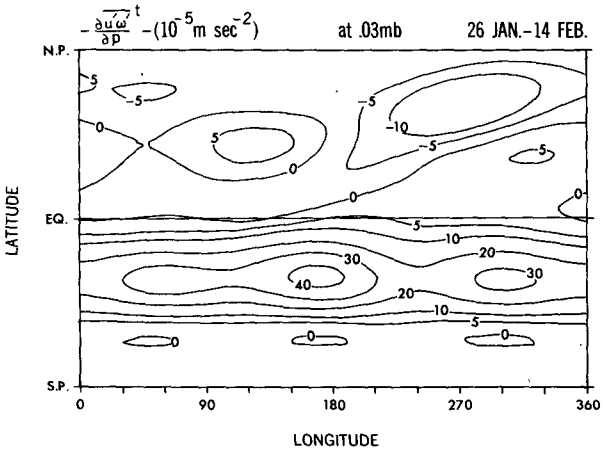

FIG. 15c. Longitude–latitude distribution of the convergence of zonal momentum flux (10^{-5} m s^{-2}) at 0.03 mb.

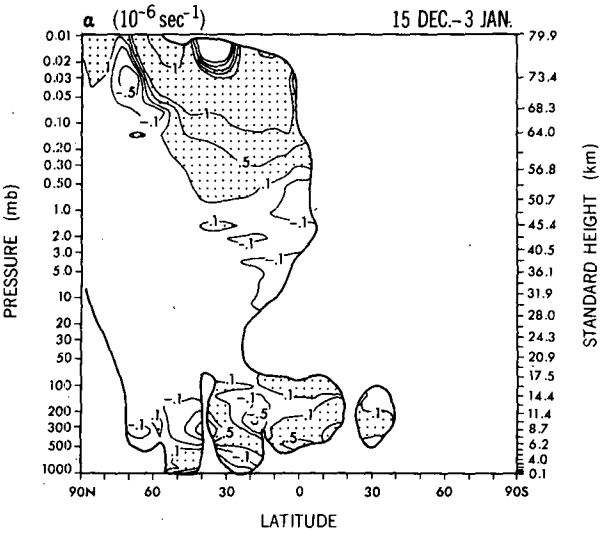

FIG. 16a. Latitude–height distribution of the equivalent Rayleigh friction coefficient for the PI period. The values are shown only when the longitudinal maximum of the zonal wind perturbation exceeds 10 m s^{-1}.

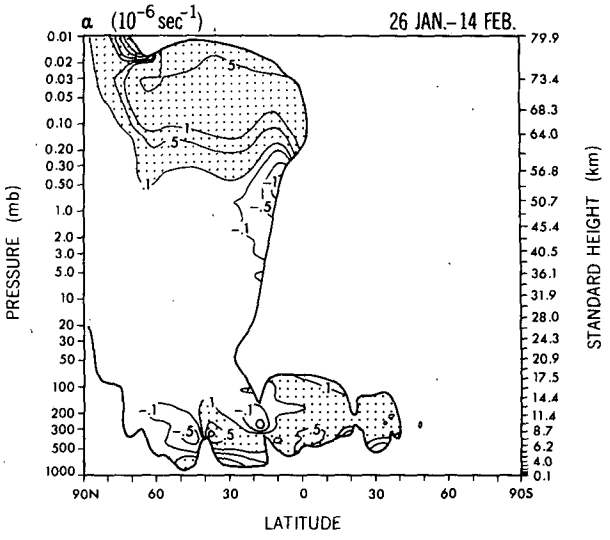

FIG. 16b. As in Fig. 16a except for the distribution for the PII period.

cients α for the PI and PII periods, respectively. The values of α are shown only when the longitudinal maximum of the zonal wind component of planetary waves u' exceeds 10 m s^{-1}, because the definition of α is not very meaningful for small u'. In both periods α is positive (frictionlike) in the mesosphere and increases with height. In the PII period, the effective damping time is about two days in the upper mesosphere. This value of α is smaller than that given by a modeling of gravity wave–planetary wave interaction (Miyahara, 1985), except in the upper mesosphere. Relative to real atmosphere, it is probably an underestimate.

It should be cautioned that the present model has strong Rayleigh friction for waves at the top level of the model in order to prevent a spurious reflection. Thus, it is probable that the momentum convergence due to wave dissipation near the top of the model is excessive for the part of the wave spectrum resolved by the model.

c. *Three-dimensional propagation of gravity waves*

In Figs. 15b and 15c, we can also recognize spatial variations of zonal momentum flux and its convergence in the Southern Hemisphere. Unlike in the Northern Hemisphere, the cause of these variations cannot be attributed to the zonal wind variations, since they are almost nonexistent (Fig. 15a). Figures 17a–c show the longitude–latitude distributions during PII of the spatially smoothed time-mean vertical flux of zonal momentum consisting of higher wavenumber components ($5 \leq k \leq 50$, $5 \leq l \leq 50$) at 0.05 mb ($\approx$70 km), 2.83 mb ($\approx$40 km) and 459.08 mb ($\approx$5 km), respectively. Horizontal spatial smoothing is accomplished by the wavenumber filter with wide wavenumber range (k = 0–9) in order to trace gravity wave packets. In the low latitudes of the troposphere (Fig. 17c) we can recognize three positive flux regions over Africa, Indonesia and South America marked as A, B and C, although positive fluxes are not dominant at this height. These positive flux regions shift toward the southeast direction and increase their magnitudes with height. We can trace these three large positive flux regions up to 70 km. Thus it seems that westerly momentum flux in the model mesosphere of the Southern Hemisphere has its origin in the tropospheric low latitude region and that the spatial variations at 70 km height are due to nonzonal distributions of the gravity wave sources in the troposphere. These interpretations are consistent with the E–P flux analysis (Fig. 7c and Fig. 8c), which shows that the E–P flux vectors in the upper stratosphere and the mesosphere of the Southern Hemisphere are directed toward the low latitudes of the troposphere through the easterlies. It should be remarked that the direction of E–P flux is the opposite of energy flux when the relative phase velocity is eastward. Figures 17a–c also suggest the possibility that in the Northern Hemisphere the westerly (positive) momentum flux over eastern Asia at 40 and 70 km height (marked as D) may partly come from the low-latitude troposphere (B) through the easterly zonal wind regions due to planetary waves, while the easterly (negative) flux over North America has its origin in the midlatitude troposphere. These interpretations are consistent with the global distribution of the zonal momentum flux (Fig. 8a).

It may be noteworthy that the propagation of eastward-moving gravity waves with westerly momentum fluxes into the summer and the winter upper mesosphere through the easterly regions seems to be some-

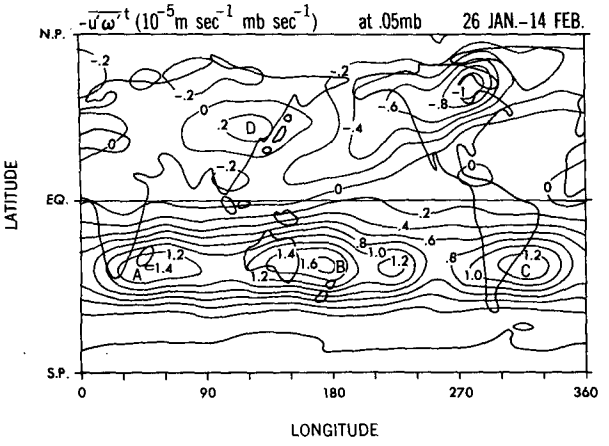

FIG. 17a. As in Fig. 15b except for the wavenumber range (k = 0–9) of the space filter at 0.05 mb.

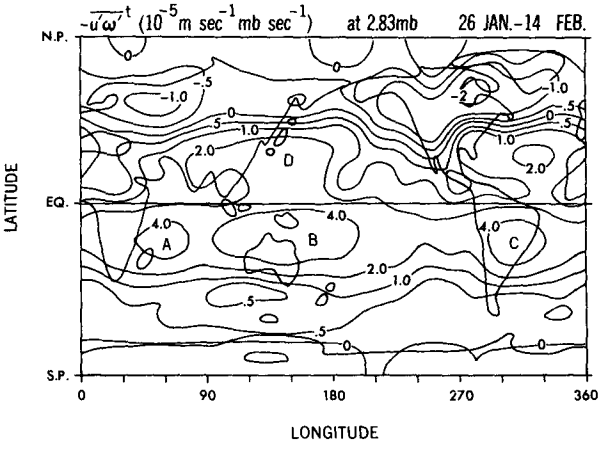

FIG. 17b. As in Fig. 17a except for the distribution at 2.83 mb.

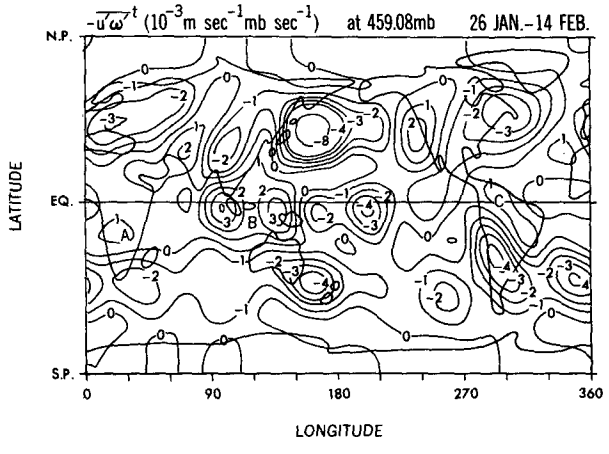

FIG. 17c. As in Fig. 17a except for the distribution at 459.08 mb.

what different from the usual waveguide propagation, which is due to a reflection and a refraction (e.g., Dickinson, 1968; Matsuno, 1970; Karoly and Hoskins, 1982). In the present case, many rays originate from their localized source region in different directions and each ray can be straight. However, the dissipation rate differs with the directions of rays, depending on the magnitude of local mean zonal winds. As a result of this differential dissipation rate, rays of slow westward-moving gravity waves and slow eastward-moving gravity waves, which are directed toward a relatively weak easterly, are dissipated in the stratosphere; only rays that are directed toward a strong easterly region can penetrate into the upper mesosphere.

5. Conclusions and remarks

Effects of gravity waves on planetary scale flow in the middle atmosphere have been analyzed by the use of bihourly sampled output data of the GFDL seasonal "SKYHI" GCM (3° lat) for Northern Hemisphere winter conditions. A preliminary analysis of gravity waves in a current high resolution (1° lat) model has also been conducted. The following results have been obtained:

1) In the stratosphere and the mesosphere, internal gravity waves in the mean zonal westerlies (easterlies) mainly consist of westward (eastward)-moving components, and carry easterly (westerly) momentum upward.

2) The dominant period of these waves is about 0.5–1.0 day for all zonal wavenumbers and the dominant phase velocity is about ± 10 m s^{-1} at $k \sim 40$ and about ± 40 m s^{-1} at $k \sim 10$. The range of vertical wavelengths inferred from the gravity wave dispersion relation is 20–50 km.

3) The vertical convergence of the mean zonal momentum flux due to these gravity waves acts to decelerate the background mean zonal winds in the upper mesosphere. The maximum deceleration rate in the summer upper mesosphere is about 30×10^{-5} m s^{-2}, while in the winter upper mesosphere it is about -30×10^{-5} m s^{-2} before the sudden warming, and it is about -7×10^{-5} m s^{-2} after the sudden warming occurs.

4) The gravity wave momentum convergence in the 3° lat model accounts for 30%–50% of the EPFD in the model winter mesosphere, while it accounts for most of the EPFD in the summer upper stratosphere and mesosphere. In the real atmosphere, the gravity wave contribution is probably even larger. The E–P flux suggests that in the summer hemisphere gravity wave energy propagates not only upward but also poleward from the equatorial troposphere.

5) The vertical momentum flux and its convergence due to gravity waves in the 1° lat model in November

are two to five times larger than those in the 3° lat model in winter.

6) The increase of the gravity waves in the 1° lat model is not only due to the addition of the higher wavenumber parts not resolved by the 3° lat model, but also to an increase of the power of the wavenumber components resolved by the 3° lat model.

7) Vertical propagation of internal gravity waves is affected not only by mean zonal winds, but also by zonal velocity perturbations associated with quasi-stationary planetary waves.

8) The drag force due to internal gravity waves acts to suppress the zonal wind component of stationary planetary waves in the winter mesosphere.

One of the interesting aspects of the present results is that the simulated gravity waves are associated with a rather narrow frequency range, while their wavenumber range is very wide. The simulated periods are roughly consistent with the observational estimates of large-scale gravity wave periods of 20–50 h according to Maekawa et al. (1984) and 10 h according to Fritts et al. (1984). However, it should be noted that there is a possibility that the frequency range of the small scale waves is affected by the insufficient model resolution. Conclusion 5 does not necessarily imply that the winter EPFD in the 1° lat model is almost entirely due to gravity waves, since the EPFD due to planetary waves also increases in this model.

The present results demonstrate that a very distinct selective transmission of internal gravity waves occurs in the present model, as expected from theoretical works (Lindzen, 1981; Matsuno, 1982; Schoeberl and Strobel, 1984; Dunkerton, 1984), and that internal gravity waves play an important role in the mesospheric circulation of the present model in a systematic way. However, a further analysis shows that there is no clear relation between the meridional wind component of planetary waves and the meridional momentum flux due to gravity waves $-\overline{v'\omega'}^{\lambda}$, as expected from a gravity wave parameterization (Miyahara, 1985). The cause of this discrepancy is under investigation.

Although effects of gravity waves on the mesospheric circulation of the present 3° lat model are significant, they are almost certainly smaller than those acting in the real stratosphere and the mesosphere (e.g., Hamilton, 1983). A cause of the insufficiency of the drag forces can be attributed to the coarse resolution of the present model. In the present models, gravity waves whose horizontal wavelengths are shorter than about 1000 km (3° lat model) and about 350 km (1° lat model) cannot be resolved properly. In the vertical direction, gravity waves whose vertical wavelengths are shorter than about 20 km cannot be resolved properly in the mesosphere of the present model. Recent observations (see a review by Fritts, 1984) suggest that the resolutions of the present models are not sufficient to obtain the entire gravity wave drag force in the atmosphere. Nevertheless, it is encouraging that the model's high frequency oscillations are characterized by physically consistent gravity waves rather than computational noise.

Since it is extremely difficult to increase the horizontal resolution further than 1°, it is necessary to develop proper parameterizations of the effects of unresolved gravity waves on the middle atmosphere circulation. The present study suggests that such a parameterization should take into account the three-dimensional propagation of gravity wave packets into nonzonal flows and the existence of a wide spectrum of gravity waves. These effects are neglected in the currently available parameterizations.

It should be also remarked that in the present model we assume a Rayleigh friction for waves at the top level of the model in order to prevent a spurious reflection, so that an excess momentum convergence due to wave dissipation may occur at the top of the model. In order to avoid this excess, we need a higher top boundary than currently available in the model.

Acknowledgments. The authors are very grateful to S. B. Fels, I. M. Held, Y. Kurihara, R. T. Pierrehumbert and J. T. Bacmeister for their valuable comments and discussions, and to D. G. Golder and L. Umscheid for their scientific assistance. Thanks are also due to P. Tunison and J. Connor for technical support.

The Geophysical Fluid Dynamics Program is supported by NOAA/Princeton University Grant NA84EAD00057.

APPENDIX

The Gravity Wave E–P Flux

For inertio-gravity waves $\overline{v'T'}^{\lambda}$ is related to $-\overline{u'\omega'}^{\lambda}$ (e.g., Andrews, 1980) as

$$\overline{v'T'}^{\lambda} = -\frac{N^2}{\hat{\omega}^2} f \overline{u'\omega'}^{\lambda}. \tag{A1}$$

Thus, the vertical component of the gravity wave E–P flux (EPF) is related to $-\overline{u'\omega'}^{\lambda}$ as follows

$$\mathrm{EPF} \equiv -\overline{u'\omega'}^{\lambda} - f\overline{v'T'}^{\lambda}/N^2 \tag{A2}$$

$$= -(1 - f^2/\hat{\omega}^2)\overline{u'\omega'}^{\lambda} \tag{A3}$$

where v' represents the meridional velocity perturbation, T' the temperature perturbation, N the Brunt–Väisälä frequency, $\hat{\omega}$ the Doppler-shifted wave frequency and f the Coriolis parameter. Thus, if $\hat{\omega}^2 \gg f^2$ is satisfied, $-\overline{u'\omega'}^{\lambda}$ can be considered as approximating the vertical component of the E–P flux. Representative Doppler-shifted frequency of the vertically propagating gravity waves in the model upper mesosphere (Figs. 3a and 3b) is estimated to be about 1.9×10^{-4} s^{-1} at $k \sim 5$, about 2.8×10^{-4} s^{-1} at $k \sim 10$, and about 8.5

$\times 10^{-4}$ s^{-1} at $k \sim 40$. These frequencies give $f^2/\hat{\omega}^2$ 0.29, 0.13 and 0.014, respectively. This means that the neglect of the heat flux term is not crucial for the waves $k \geq 5$. Thus, we use $-\overline{u'\omega'}^{\lambda}$ as a first approximation.

REFERENCES

Andrews, D. G., 1980: On the mean motion induced by transient inertio-gravity waves. *Pure Appl. Geophys.*, **118,** 177–188.

——, and M. E. McIntyre, 1976: Planetary waves in horizontal and vertical shear: The generalized Eliassen–Palm relation and the mean zonal acceleration. *J. Atmos. Sci.*, **33,** 2031–2048.

——, J. D. Mahlman and R. W. Sinclair, 1983: Eliassen–Palm diagnostics of wave–mean flow interaction in the GFDL "SKYHI" general circulation model. *J. Atmos. Sci.*, **40,** 2768–2784.

Dickinson, R. E., 1968: Planetary Rossby waves propagating vertically through weak westerly wind wave guides. *J. Atmos. Sci.*, **25,** 984–1002.

Dunkerton, T. J., 1984: Inertia–gravity waves in the stratosphere. *J. Atmos. Sci.*, **41,** 3396–3404.

——, and N. Butchart, 1984: Propagation and selective transmission of internal gravity waves in a sudden warming. *J. Atmos. Sci.*, **41,** 1443–1460.

Fels, S. B., 1984: The radiative damping of short vertical scale waves in the mesosphere. *J. Atmos. Sci.*, **41,** 1755–1764.

——, 1985: Radiative-dynamical interactions in the middle atmosphere. *Advances in Geophysics,* Vol. 28, Part A, Academic Press, 591 pp.

——, J. D. Mahlman, M. D. Schwarzkopf and R. W. Sinclair, 1980: Stratospheric sensitivity to perturbations in ozone and carbon dioxide: Radiation and dynamical response. *J. Atmos. Sci.*, **37,** 2265–2297.

Fritts, D. C., 1984: Gravity wave saturation in the middle atmosphere: A review of theory and observations. *Rev. Geophys. Space Phys.*, **22,** 275–308.

——, B. B. Balsley and W. L. Ecklund, 1984: VHF echoes from the arctic mesosphere and lower thermosphere, part II, Interpretations. *Dynamics of the Middle Atmosphere,* J. R. Holton and T. Matsuno, Eds., Terra Scientific, 97–115.

Hamilton, K., 1983: Diagnostic study of the momentum balance in the Northern Hemisphere winter stratosphere. *Mon. Wea. Rev.*, **111,** 1434–1441.

Hayashi, Y., 1982: Space–time spectral analysis and its applications to atmospheric waves. *J. Meteor. Soc. Japan,* **60,** 156–171.

——, 1985: Theoretical interpretations of the Eliassen–Palm diagnostics of wave–mean flow interaction. Part I: Effects of the lower boundary, Part II: Effects of mean damping. *J. Meteor. Soc. Japan,* **63,** 497–512, 513–521.

——, D. G. Golder and J. D. Mahlman, 1984: Stratospheric and mesospheric Kelvin waves simulated by the GFDL "SKYHI" general circulation model. *J. Atmos. Sci.*, **41,** 1971–1984.

Holton, J. R., 1982: The role of gravity wave-induced drag and diffusion in the momentum budget of the mesosphere. *J. Atmos. Sci.*, **39,** 791–799.

——, 1983: The influence of gravity wave breaking on the general circulation of the middle atmosphere. *J. Atmos. Sci.*, **40,** 2497–2507.

——, and W. M. Wehrbein, 1980: A numerical model of the zonal mean circulation of the middle atmosphere. *Pure Appl. Geophys.*, **118,** 284–306.

Houghton, J. T., 1978: The stratosphere and mesosphere. *Quart. J. Roy. Meteor. Soc.*, **104,** 1–28.

Karoly, J. D., and B. J. Hoskins, 1982: Three-dimensional propagation of planetary waves. *J. Meteor. Soc. Japan,* **60,** 109–123.

Kida, H., 1984: A numerical experiment on the general circulation of the middle atmosphere with a three-dimensional model explicitly representing internal gravity waves and their breaking. *Pure Appl. Geophys.*, **122,** 731–746.

Kurihara, Y., 1965: On the use of implicit and iterative methods for the time integration of the wave equation. *Mon. Wea. Rev.*, **93,** 33–46.

Leovy, C. B., 1964: Simple models of thermally driven mesospheric circulation. *J. Atmos. Sci.*, **25,** 327–341.

Levy, H., II, J. D. Mahlman and W. J. Moxim, 1982: Tropospheric N_2O variability. *J. Geophys. Res.*, **87,** 3061–3080.

Lindzen, R. S., 1981: Turbulence and stress due to gravity wave and tidal breakdown. *J. Geophys. Res.*, **86,** 9707–9714.

——, 1984: Gravity waves in the mesosphere. *Dynamics of the Middle Atmosphere,* J. R. Holton and T. Matsuno, Eds., Terra Scientific, 3–18.

——, and C.-Y. Tsay, 1975: Wave structure of the tropical stratosphere over the Marshall Islands area during 1 April–1 July 1958. *J. Atmos. Sci.*, **32,** 2008–2021.

Maekawa, Y., S. Fukao, T. Sato, S. Kato and R. Woodman, 1984: Internal inertio–gravity waves in the tropical lower stratosphere observed by the Arecibo radar. *J. Atmos. Sci.*, **41,** 2359–2367.

Mahlman, J. D., and L. J. Umscheid, 1984: Dynamics of the middle atmosphere: Successes and problems of the GFDL "SKYHI" general circulation model. *Dynamics of the Middle Atmosphere,* J. R. Holton and T. Matsuno, Eds., Terra Scientific, 501–525.

Matsuno, T., 1970: Vertical propagation of stationary planetary waves in the winter Northern Hemisphere. *J. Atmos. Sci.*, **27,** 871–883.

——, 1982: A quasi one-dimensional model of the middle atmosphere circulation interacting with internal gravity waves. *J. Meteor. Soc. Japan,* **60,** 215–226.

Miyahara, S., 1984: A numerical simulation of the zonal mean circulation of the middle atmosphere including effects of solar diurnal tidal waves and internal gravity waves: Solstice condition. *Dynamics of the Middle Atmosphere,* J. R. Holton and T. Matsuno, Eds., Terra Scientific, 271–287.

——, 1985: Suppression of stationary planetary waves by internal gravity waves in the mesosphere. *J. Atmos. Sci.*, **42,** 100–107.

Schoeberl, M. R., and D. F. Strobel, 1978: The zonally averaged circulation of the middle atmosphere. *J. Atmos. Sci.*, **35,** 579–591.

——, and ——, 1984: Nonzonal gravity wave breaking in the winter mesosphere. *Dynamics of the Middle Atmosphere,* J. R. Holton and T. Matsuno, Eds., Terra Scientific, 45–64.

Smith, A. K., and L. V. Lyjak, 1985: An observational estimate of gravity wave drag from the momentum balance in the middle atmosphere. *J. Geophys. Res.*, **90,** 2233–2241.

Vincent, R. A., and I. M. Reid, 1983: HF Doppler measurements of mesospheric gravity wave momentum fluxes. *J. Atmos. Sci.*, **40,** 1321–1333.